Alternative Total Lagrangian Formulations for Corrected Smooth Particle Hydrodynamics (CSPH) Methods in Large Strain Dynamic Problems

Javier Bonet — Sivakumar Kulasegaram

Department of Civil Engineering
University of Wales Swansea, Swansea SA2 8PP, UK
j.bonet@swansea.ac.uk

ABSTRACT. *This paper discusses alternative Lagrangian formulations for smooth particle hydrodynamics method. These Lagrangian formulations are here employed in solving large strain problems that involve elasto-plastic and hyperelastic materials. It has previously been shown in the literature that the Lagrangian formulation for continuum eliminates the problem of tension instability which is generally coupled with Eulerian continuum formulation of smooth particle hydrodynamics and other meshless methods. This paper presents the details of the methodologies used in formulating Lagrangian smooth particle hydrodynamics method and their characteristics.*

RÉSUMÉ. *Dans cet article, nous discutons les formulations lagrangiennes alternatives pour la méthode SPH. Ces formulations lagrangiennes sont utilisées ici pour la résolution des problèmes des grandes déformations qui incluent les matériaux élasto-plastiques et hyper-élastiques. Il a été démontré dans la littérature, que la formulation lagrangienne du continuum élimine le problème d'instabilité en traction, qui est généralement associé avec la formulation eulérienne de la méthode SPH et d'autres méthodes sans maillage. Cet article présente les détails des méthodologies utilisées dans la formulation de la méthode lagrangienne SPH et les caractéristiques associées.*

KEYWORDS: *meshless methods; SPH; CSPH; large deformation; Lagrangian SPH.*

MOTS-CLÉS : *méthodes sans maillage, SPH, CSPH, grandes déformations, SPH Lagrangienne.*

REEF – 11/2002. Meshfree Computational Mecanics, pages 893 to 912

1. Introduction

The smooth particle hydrodynamics (SPH) is truly meshfree, simple and robust computational technique that can be used in numerical simulations of various engineering problems. The method was pioneered in 1977 for modelling astrophysical and cosmological problems, and since the early 90's the application has been extended to numerous areas of computational mechanics [1-10]. However, in spite of its attraction for computational mechanics, the method suffers from lack of accuracy and more importantly instability from lack of nodal completeness and/or integrability of the approximations for functions and their derivatives. Recently, a number of techniques have been developed to circumvent such difficulties encountered in SPH and other meshless methods [10-15].

One of the major obstacles generally faced in meshless methods such as SPH is the presence of tensile instability in the formulation of solid applications [11-15]. It has been reported that the tensile instability is to a large extent associated with using Eulerian kernels [12], where the derivatives of the kernel functions are constantly changing as the particles move. The changes in the internal forces brought about by these changes in the derivatives of the Eulerian kernels give rise to spurious terms in the tangent stiffness of the system which are the main cause of the so called tension instability [12]. A number of techniques have been developed to address this issue in the case of SPH and related meshfree methods [11,12,15]. One of such techniques is based on formulating Lagrangian continuum equations whereby the internal forces are evaluated with respect to a fixed reference configuration. In this case the kernel function and its derivatives are based at the reference configuration and hence do not depend on the current position of the particles [11,12]. Thus the tensile instability will be completely eliminated or transformed into spurious mechanisms, which can be easily controlled by the use of artificial viscosity. The detailed analysis of tensile instability and alternative approaches to eliminate these instabilities can be found in the literature [11-15]. This paper mainly dwells on two different ways of formulating SPH in a Lagrangian setting and compares their salient features. Several numerical examples are presented to demonstrate the ability of the formulations to simulate complex problems.

2. Numerical methodology

2.1. *SPH Approximations*

In meshfree methods such as SPH, any problem variable and its gradient are generally interpolated from values at a discrete number of particles by using the following approximations:

$$\phi(\boldsymbol{x}) = \sum_{b=1}^{N} V_b \phi_b W_b(\boldsymbol{x}) \tag{1}$$

$$\nabla\phi(\boldsymbol{x}) = \sum_{b=1}^{N} V_b \phi_b \nabla W_b(\boldsymbol{x}) \tag{2}$$

where V_b denotes the volume of material associated to a given particle and W_b represents the 'kernel' or interpolation function, which usually has a bell shape with a compact support as shown in Figure 1.

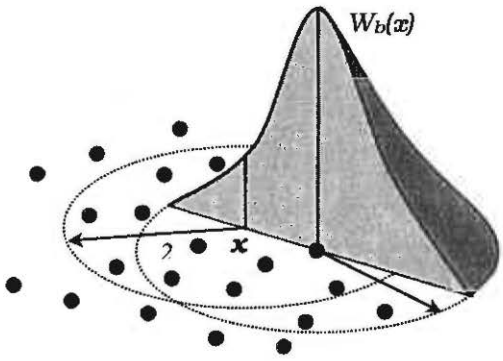

Figure 1. *Particle interpolation and kernel function*

Most commonly used kernel function in SPH is a cubic spline kernel function given by,

$$W(x) = \frac{c}{h^d}\begin{cases} 1 - \dfrac{3}{2}\xi^2 + \dfrac{3}{4}\xi^3 & \text{if } \xi \le 1 \\ \dfrac{1}{4}(2-\xi)^3 & \text{if } 1 < \xi \le 2 \\ 0 & \text{if } \xi > 2 \end{cases} \quad ; \quad \xi = \frac{\|\boldsymbol{x}\|}{h} \tag{3}$$

where d is the number of dimensions of the problem and c is a scaling factor to normalise the kernel function. Here, the length parameter h has a similar interpretation to the element size in finite element method. For instance, applying equation (1) to density of a continuum leads to the classical SPH equation :

$$\rho(\boldsymbol{x}) = \sum_{b=1}^{N} m_b W_b(\boldsymbol{x}) \tag{4}$$

In this way, the SPH representation of the governing equations can be built from fundamental equations of motion.

2.2. *Continuum Equations*

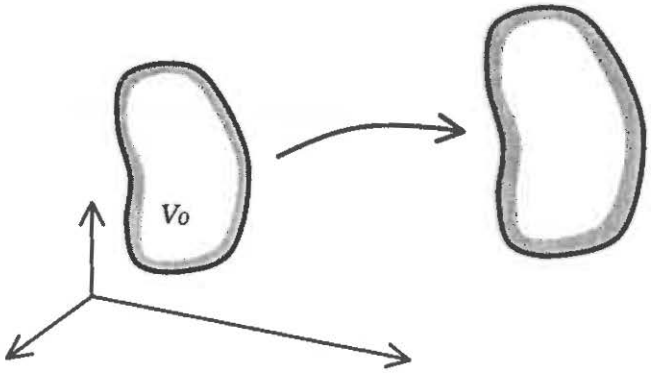

Figure 2. *Continuum deformation*

Consider a 3-dimensional continuum shown in Figure 2 undergoing a given motion defined by a mapping ϕ between initial and current position as:

$$\boldsymbol{x} = \boldsymbol{\phi}\left(\boldsymbol{X}, t\right) \tag{5}$$

which gives the position $\boldsymbol{x}$ of each material point $\boldsymbol{X}$ as a function of time. The deformation gradient $\boldsymbol{F}$ is defined as:

$$\boldsymbol{F} = \nabla_0 \boldsymbol{\phi} = \frac{\partial \boldsymbol{x}}{\partial \boldsymbol{X}} \tag{6}$$

and the Jacobian or volume ratio J of the continuum is given by:

$$J = \det \boldsymbol{F} = \frac{dV}{dV_0} \tag{7}$$

where dV_0 and dV represent the initial and the current element volumes. Conservation of mass or continuity equation is then obviously expressed as;

$$\rho_0 = \rho J \tag{8}$$

where ρ_0 and ρ are initial and current densities of volume elements.

The momentum balance equation for the deformable body is given by,

$$\rho_0 \boldsymbol{a} = \rho_0 \boldsymbol{f}_0 + \nabla_0 \boldsymbol{P} : \boldsymbol{I} \tag{9}$$

where $\boldsymbol{a}$ is acceleration, $\boldsymbol{f}_0$ is body force per unit mass, typically due to gravity $\boldsymbol{g}$ and $\boldsymbol{P}$ is first Piola-Kirchhoff tensor. The first Piola-Kirchoff tensor can be expressed in terms of Cauchy stress tensor as,

$$\boldsymbol{P} = J\boldsymbol{\sigma}\boldsymbol{F}^{-T} \tag{10}$$

And finally, in the absence of heat transfer, the conservation of energy of the continuum can be written by,

$$\rho_0 \dot{E} = \boldsymbol{P} : \dot{\boldsymbol{F}} \tag{11}$$

where E is the internal energy per unit mass. As the analyses in this paper will be confined to isothermal, adiabatic processes the terms corresponding to heat energy have been ignored in the above energy conservation equation. The following section deals with discretization of the governing equations based on Lagrangian SPH formulations.

2.3. *Discrete equilibrium equations*

In order to discretise the equilibrium equation (9), a standard Galerkin approach is employed, which leads to the principle of virtual work expressed as,

$$\delta \dot{w}_{\text{ine}} = \delta \dot{w}_{\text{ext}} - \delta \dot{w}_{\text{int}} \tag{12}$$

where using standard mass lumping the inertia and external (gravity due) virtual work rates are expressed in terms of particle masses, accelerations and virtual velocities as:

$$\delta \dot{w}_{\text{ine}} = \sum_I m_I \boldsymbol{a}_I \cdot \delta \boldsymbol{v}_I; \quad \delta \dot{w}_{\text{ext}} = \sum_I m_I \boldsymbol{g} \cdot \delta \boldsymbol{v}_I \tag{13}$$

and the internal virtual work will be expressed in following section in terms of the internal equivalent forces as,

$$\delta \dot{w}_{\text{int}} = \int_{V_0} \boldsymbol{P} : \delta \dot{\boldsymbol{F}} \, dV_0 = \sum_I \boldsymbol{T}_I \cdot \delta \boldsymbol{v}_I \tag{14}$$

The standard dynamic equilibrium equation for a given particle is then obtained as,

$$m_I \boldsymbol{a}_I = m_I \boldsymbol{g} - \boldsymbol{T}_I \tag{15}$$

3. Lagrangian SPH

Previous research has revealed that the discretisation of the continuum equations based on the framework of a fully Lagrangian formulation eliminates undesirable effects due to tensile instabilities [12]. In Lagrangian SPH all derivatives are taken with respect to a constant reference configuration where both the kernel and its derivatives remain constant. In this section two different Lagrangian formulations, one based on Corrected SPH formulation and another based on traditional SPH formulation are described.

3.1. *Corrected SPH Formulation*

Consider a general deformation of a body discretised using number of SPH particles as shown in Figure 3. The deformation gradient defined by equation (6) can now be evaluated at a given particle I in terms of the current particle positions as:

$$\boldsymbol{F}_I = \nabla_0 \boldsymbol{\phi} = \sum_{J=1}^{N} \boldsymbol{x}_J \otimes \boldsymbol{G}_J \left(\boldsymbol{X}_I \right) \tag{16}$$

where the gradient functions $\boldsymbol{G}$ contain the corrected kernel gradients $\tilde{\nabla} W \left(\boldsymbol{X} \right)$ at the initial reference configuration, that is:

$$\boldsymbol{G}_K \left(\boldsymbol{X}_I \right) = V_K \tilde{\nabla}_0 W_K \left(\boldsymbol{X}_I \right) \tag{17}$$

Possible ways of correcting the above kernel or its gradient that will ensure linear completeness are discussed in references [9-11]. Note that the necessary correction will be performed at the initial reference configuration of the body.

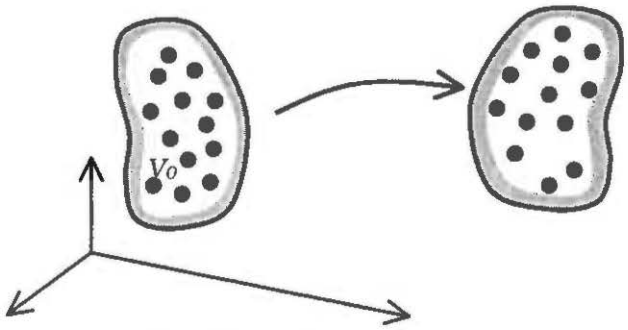

Figure 3. *General deformation from reference to current*

In order to derive general equations for the internal forces using a Lagrangian corrected SPH technique, consider the internal virtual work equation expressed in the reference configuration in terms of the first Piola-Kirchoff tensor $\boldsymbol{P}$ as,

$$\delta \dot{w}_{\text{int}} = \int_{V_0} \boldsymbol{P} : \delta \dot{\boldsymbol{F}} \, dV_0 = \sum_{J=1}^{N} V_J^0 \boldsymbol{P}_J : \delta \dot{\boldsymbol{F}}_J \tag{18}$$

The virtual deformation gradient rate emerges from equation (16) as:

$$\delta \dot{\boldsymbol{F}}_J = \sum_{K=1}^{N} \delta \boldsymbol{v}_K \otimes \boldsymbol{G}_K \left(\boldsymbol{X}_J \right) \tag{19}$$

which, upon substitution into equation (18) yields the virtual internal work expression as:

$$\begin{aligned}\delta \dot{w}_{\text{int}} &= \sum_{J=1}^{N} V_J^0 \boldsymbol{P}_J : \delta \dot{\boldsymbol{F}}_J \\ &= \sum_{J=1}^{N} V_J^0 \boldsymbol{P}_J : \left(\sum_{K=1}^{N} \delta \boldsymbol{v}_K \otimes \boldsymbol{G}_K \left(\boldsymbol{X}_J \right) \right) \\ &= \sum_{K=1}^{N} \delta \boldsymbol{v}_K \cdot \left(\sum_{J=1}^{N} V_J^0 \boldsymbol{P}_J \boldsymbol{G}_K \left(\boldsymbol{X}_J \right) \right)\end{aligned} \tag{20}$$

thus enabling the internal force vector corresponding to a given node I to be easily identified from this expression as:

$$\boldsymbol{T}_I = \sum_{J=1}^{N} V_J^0 \boldsymbol{P}_J \boldsymbol{G}_I \left(\boldsymbol{X}_J \right) \tag{21}$$

The obvious advantage of using this equation for the evaluation of internal forces in a discretized continuum is the fact that the kernel derivative functions $\boldsymbol{G}$ are fixed at the initial (or reference) configuration and hence will not be dependent upon current nodal positions. In addition it can be noted that the corrections also evaluated at the initial configuration thus enable to reduce the computational cost.

3.2. *Alternative SPH Formulation*

The previous formulation relies on linearly corrected kernel gradient vectors obtained in the initial configuration. An alternative simpler formulation, which leads to equations similar to the traditional SPH is presented in this section.

Consider first the approximation of the deformation gradient tensor $\boldsymbol{F}$. Given that this is a two point tensor relating initial vectors $d\boldsymbol{X}$ to their final counterparts $d\boldsymbol{x} = \boldsymbol{F} d\boldsymbol{X}$, a simple approximation at a given particle I is given by the weighted average of dyadic (tensor) products of incremental vectors as:

$$\boldsymbol{F}_I = \left(\sum_{J=1}^{N} m_I W_{IJ} \left(\boldsymbol{x}_J - \boldsymbol{x}_I \right) \otimes \left(\boldsymbol{X}_J - \boldsymbol{X}_I \right) \right) \boldsymbol{M}_I^{-1} \tag{22}$$

where W_{IJ} denotes the uncorrected derivative of the kernel with respect to particle distance as,

$$W_{IJ} = \frac{1}{r_{IJ}} \frac{dW_I(\boldsymbol{X}_J)}{dr_{IJ}}; \quad r_{IJ}^2 = (\boldsymbol{X}_J - \boldsymbol{X}_I) \cdot (\boldsymbol{X}_J - \boldsymbol{X}_I) \tag{23}$$

and the correction matrix $\boldsymbol{M}$ is chosen so that for the case with uniform deformation gradient, where $\boldsymbol{x}_J - \boldsymbol{x}_I = \boldsymbol{F}(\boldsymbol{X}_J - \boldsymbol{X}_I)$, the exact deformation gradient is found. A simple substitution shows that this matrix must consequently be given by;

$$\boldsymbol{M}_I = \sum_{J=1}^{N} W_{IJ} m_J (\boldsymbol{X}_J - \boldsymbol{X}_I) \otimes (\boldsymbol{X}_J - \boldsymbol{X}_I) \tag{24}$$

In order to derive the corresponding equations for internal forces based on the above alternative formulation, consider again the internal virtual work equation as;

$$\delta \dot{w}_{\text{int}} = \sum_{I=1}^{N} m_I \frac{\boldsymbol{P}_I}{\rho_I^0} : \delta \dot{\boldsymbol{F}}_I \tag{25}$$

where the virtual deformation gradient rate is now derived from equation (22) to give:

$$\delta \dot{\boldsymbol{F}}_I = \left(\sum_{J=1}^{N} W_{IJ} m_J (\delta \boldsymbol{v}_J - \delta \boldsymbol{v}_I) \otimes (\boldsymbol{X}_J - \boldsymbol{X}_I) \right) \boldsymbol{M}_I^{-1} \tag{26}$$

Substituting the above equation into the virtual work expression gives,

$$\delta \dot{w}_{\text{int}} = \sum_{I,J=1}^{N} W_{IJ} m_I m_J \frac{\boldsymbol{P}_I \boldsymbol{M}_I^{-1}}{\rho_I^0} : (\delta \boldsymbol{v}_J - \delta \boldsymbol{v}_I) \otimes (\boldsymbol{X}_J - \boldsymbol{X}_I) \tag{27}$$

After simple algebra the above expression can be re-written as:

$$\delta \dot{w}_{\text{int}} = \sum_{K=1}^{N} \delta \boldsymbol{v}_K \cdot \left(\sum_{L=1}^{N} m_K m_L W_{LK} \frac{\boldsymbol{P}_L \boldsymbol{M}_L^{-1}}{\rho_L^0} + m_K m_L W_{KL} \frac{\boldsymbol{P}_K \boldsymbol{M}_K^{-1}}{\rho_K^0} \right) (\boldsymbol{X}_K - \boldsymbol{X}_L) \tag{28}$$

thus enabling the internal force vector corresponding to a given node I to be easily identified from this expression as:

$$\boldsymbol{T}_I = \sum_{J=1}^{N} m_I m_J \left(W_{JI} \frac{\boldsymbol{P}_J \boldsymbol{M}_J^{-1}}{\rho_J^0} + W_{IJ} \frac{\boldsymbol{P}_I \boldsymbol{M}_I^{-1}}{\rho_I^0} \right) (\boldsymbol{X}_I - \boldsymbol{X}_J) \quad (29)$$

For the particular case where kernel functions are symmetric that is,

$$W_{IJ} = -W_{JI} \text{ and } \nabla_0 W_I(\boldsymbol{X}_J) = -\nabla_0 W_J(\boldsymbol{X}_I) = (\boldsymbol{X}_I - \boldsymbol{X}_J) W_{IJ} \quad (30)$$

the internal force $\boldsymbol{T}_I$ can be written as,

$$\boldsymbol{T}_I = \sum_{J=1}^{N} m_I m_J \left(\frac{\boldsymbol{P}_J \boldsymbol{M}_J^{-1}}{\rho_J^0} + \frac{\boldsymbol{P}_I \boldsymbol{M}_I^{-1}}{\rho_I^0} \right) \nabla_0 W_I(\boldsymbol{X}_J) \quad (31)$$

As the matrices $\boldsymbol{M}$ are fixed at the initial (or reference) configuration, the above internal force equation shares the same advantages of equation (21). In addition, the final equation for the internal forces closely resembles the equations used in standard SPH.

3.3. *Preservation of momentum*

It is essential to examine whether the Lagrangian formulations proposed in the above discussions satisfy the momentum preservation conditions usually required of a continuum equations. For this purpose internal force equations linear and angular momentum of the Lagrangian formulations are analysed. It can be recalled that linear momentum is preserved whenever the sum of the internal forces of each particle vanishes for any state of stresses, that is:

$$\sum_{I=1}^{N} \boldsymbol{T}_I = \boldsymbol{0} \quad (32)$$

In the case of corrected SPH formulation substituting for $\boldsymbol{T}_I$ from equation (21) into the above condition gives, after simple algebra,

$$\sum_{I=1}^{N} \boldsymbol{T}_I = \sum_{J=1}^{N} V_J \boldsymbol{P}_J \left(\sum_{I=1}^{N} \boldsymbol{G}_I(\boldsymbol{X}_J) \right) \quad (33)$$

From the above equation it can be stated that the conservation of linear momentum enforces the following requirement on the initial gradient vectors $\boldsymbol{G}$:

$$\sum_{I=1}^{N} \boldsymbol{G}_I\left(\boldsymbol{X}_b\right) = \boldsymbol{0} \tag{34}$$

This is simply the order zero completeness condition which ensures that the gradient of a constant function vanishes. A number of different techniques to ensure that this condition is satisfied are reported in the literature [10-12].

It is trivial to prove that the alternative SPH formulation defined in section 3.2 satisfies equation (32) and hence preserves linear momentum. In general internal force at particle I can be expressed as the sum of interaction forces between pairs of particles as (see Figure 4)

$$\boldsymbol{T}_I = \sum_{J=1}^{N} \boldsymbol{T}_{IJ} \tag{35}$$

For instance if the internal forces are given by equation (31) then the interaction force is

$$\boldsymbol{T}_{IJ} = m_I m_J \left(\frac{\boldsymbol{P}_I \boldsymbol{M}_I^{-1}}{\rho_I^0} + \frac{\boldsymbol{P}_J \boldsymbol{M}_J^{-1}}{\rho_J^0} \right) \nabla_0 W_J\left(\boldsymbol{X}_I\right) \tag{36}$$

Given that $\nabla W_I\left(\boldsymbol{X}_J\right) = -\nabla W_J\left(\boldsymbol{X}_I\right)$, it is clear that $\boldsymbol{T}_{IJ} = -\boldsymbol{T}_{JI}$, and consequently the total sum of all interaction pairs will vanish (see figure 4).

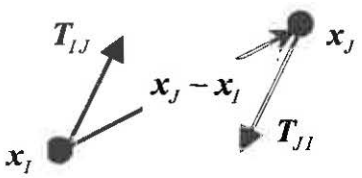

Figure 4. *Interaction forces between two particles*

Although most of the formulations will preserve linear momentum, the same is not true for angular momentum. It can be recalled that the angular momentum is

preserved when the total moment of the internal forces with respect to an arbitrary reference point vanishes, that is:

$$\sum_{I=1}^{N} \boldsymbol{x}_I \times \boldsymbol{T}_I = \boldsymbol{0} \tag{37}$$

In case of corrected SPH formulation, again introducing the internal force equation (21) gives after simple algebra:

$$\begin{aligned} \sum_{I=1}^{N} \boldsymbol{x}_I \times \boldsymbol{T}_I &= -\boldsymbol{\varepsilon} : \sum_{I=1}^{N} \boldsymbol{T}_I \otimes \boldsymbol{x}_I \\ &= -\boldsymbol{\varepsilon} : \sum_{J=1}^{N} V_J^0 \boldsymbol{P}_J \left(\sum_{I=1}^{N} \boldsymbol{G}_I (\boldsymbol{X}_J) \otimes \boldsymbol{x}_I \right) \end{aligned} \tag{38}$$

where $\boldsymbol{\varepsilon}$ denotes the third order alternating tensor. The term in brackets in the above equation coincides with the transpose of the deformation gradient tensor given by equation (16). Taking this into account together with the equation (10) relating Cauchy and Piola-Kirchhof stresses and the symmetry of $\boldsymbol{\sigma}$ gives:

$$\begin{aligned} \sum_{I=1}^{N} \boldsymbol{x}_I \times \boldsymbol{T}_I &= -\boldsymbol{\varepsilon} : \sum_{J=1}^{N} V_J^0 \boldsymbol{P}_J \boldsymbol{F}_J^T \\ &= -\boldsymbol{\varepsilon} : \sum_{J=1}^{N} V_J \boldsymbol{\sigma}_J \\ &= \boldsymbol{0} \end{aligned} \tag{39}$$

Consequently, internal force equation (21) preserves angular momentum for any choice for initial gradient vectors $\boldsymbol{G}$.

In the case of the alternative Lagrangian SPH formulation discussed in section 3.2, a similar derivation, again relying on the symmetry of the Cauchy stresses and equation (22), enables the preservation of angular momentum to be proved as,

$$\begin{aligned}\sum_{I=1}^{N} \boldsymbol{x}_I \times \boldsymbol{T}_I &= -\boldsymbol{\varepsilon} : \sum_{I=1}^{N} \boldsymbol{T}_I \otimes \boldsymbol{x}_I \\ &= -\boldsymbol{\varepsilon} : \sum_{I,J=1}^{N} m_I m_J \left(W_{JI} \frac{\boldsymbol{P}_J \boldsymbol{M}_J^{-1}}{\rho_J^0} + W_{IJ} \frac{\boldsymbol{P}_I \boldsymbol{M}_I^{-1}}{\rho_I^0} \right) (\boldsymbol{X}_I - \boldsymbol{X}_J) \otimes \boldsymbol{x}_I \\ &= -\boldsymbol{\varepsilon} : \sum_{I,J=1}^{N} m_I m_J \left(W_{JI} \frac{\boldsymbol{P}_J \boldsymbol{M}_J^{-1}}{\rho_J^0} \right) (\boldsymbol{X}_I - \boldsymbol{X}_J) \otimes (\boldsymbol{x}_I - \boldsymbol{x}_J) \\ &= -\boldsymbol{\varepsilon} : \sum_{J=1}^{N} m_J \boldsymbol{P}_J \boldsymbol{F}_J^T \\ &= -\boldsymbol{\varepsilon} : \sum_{J=1}^{N} m_J \boldsymbol{\sigma}_J \\ &= \boldsymbol{0}\end{aligned} \tag{40}$$

4. Numerical examples

In order to illustrate the ability of Lagrangian SPH formulations various numerical examples are presented in this section. The examples are targeted to demonstrate the simulations of large strain three dimensional problems involving elasto-plastic and hyperelastic materials.

4.1. *Taylor Bar Impact*

This section presents numerical results from the simulation of a small cylindrical copper bar against a rigid planar wall. The bar has an initial length of 0.0324m and initial radius 0.0032m. The Initial velocity of the bar is 227 m/s and the termination time of the problem is 80μs. Von Mises plasticity with linear isotropic hardening is employed for the numerical computation. Material properties used for copper are given in Table 1 [17]. This is a classical dynamic test example and the results obtained match closely with those achieved using a standard FE formulation [17].

Elastic Modulus E	117 GN/m^2
Poisson's Ratio ν	0.35
Yield Stress σ_y	0.4 GN/m^2
Hardening Modulus H	0.1 GN/m^2
Density ρ	8930 kg/m^3

Table 1. *Copper Bar Material Properties*

Figure 5 below shows the deformed shape and the distribution of equivalent plastic strain at various stages of the numerical simulation. The results show that the meshless method yield larger maximal equivalent plastic strain than finite elements, but the discrepancy is small.

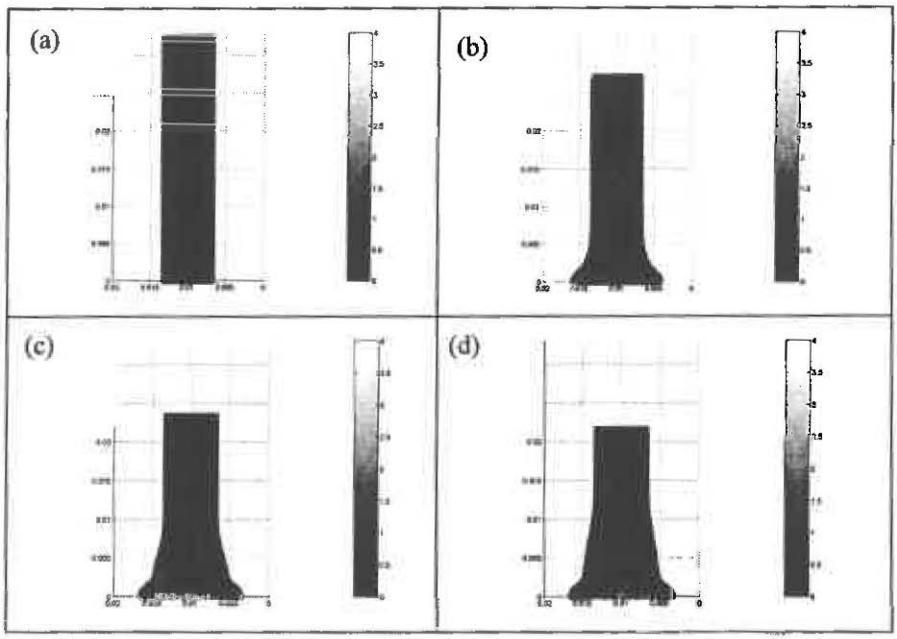

Figure 5. *Deformed shape and equivalent plastic strain of a Taylor bar at various stages*

4.2. *Bending of Hyperelastic Cylinder*

This example involves a nearly incompressible neo-Hoookean cylinder travelling with initial velocity of 1.88 m/s to the right which is suddenly fixed at its base. The initial radius is .32 m and the length 3.24 m. The shear modulus is .3571 MN/m^2 and the bulk modulus is 1.67 MN/m^2. The shapes obtained at different times are shown in Figure 6. The same example has been run using a standard dynamic FE code with identical initial nodal positions and tri-linear 8 noded cube elements. The SPH and FE solution for the centreline of the cylinder at three different times are compared in Figure 7, where the agreement can be seen to be excellent.

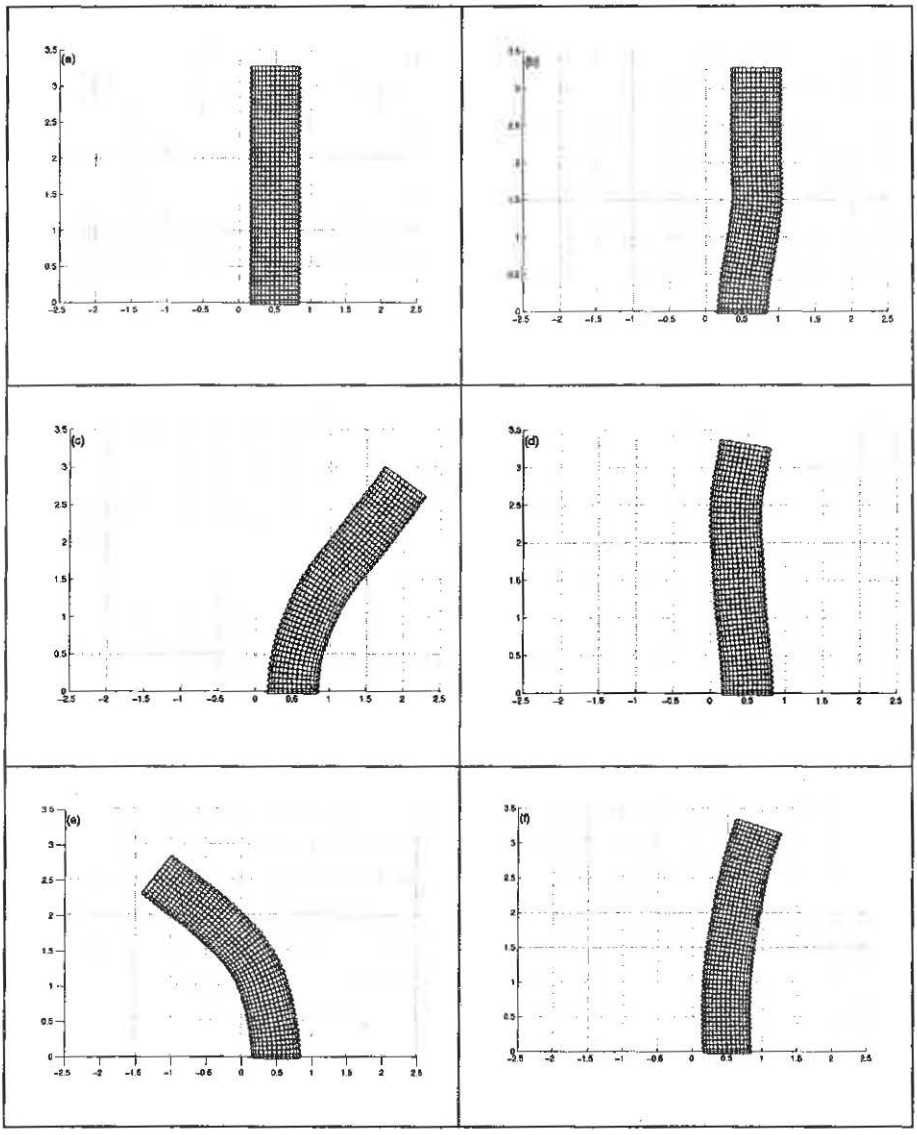

Figure 6. *Deformed shapes of the hyperelastic material at various stages*

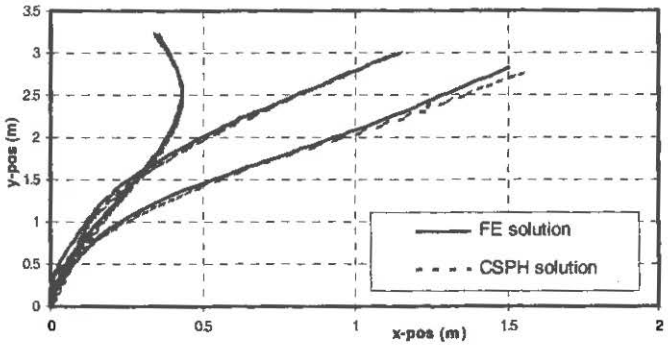

Figure 7. *FE vs. CSPH comparison for the oscillating cylinder*

4.3. *High Speed Impact of Brittle Materials*

In this section the high speed impact and fracture of Tungsten cube is simulated using Lagrangian SPH formulations. A Silica-Phenolic target panel is impacted at right angle with Tungsten cube as described in Figure 8. The numerical computation is performed for a 42.2 g Tungsten cube travelling at 1930 m/s before striking a long stationary bar made of Silica-Phenolic material.

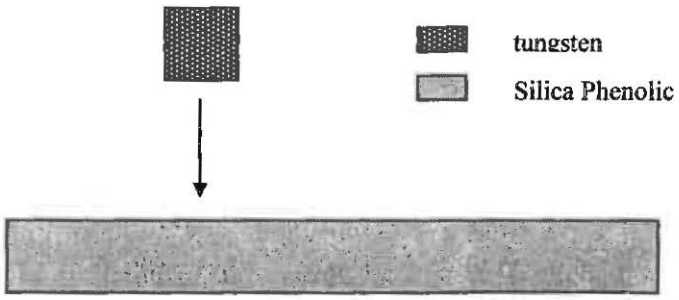

Figure 8. *Schematic diagram of the numerical experiment*

In addition to the governing equations discussed in section 2.2, the pressure equation incorporating specific internal energy are used in the computation. For this purpose, the pressure is evaluated by using Mie-Gruneisen equation of state given as [6,18],

$$P = \left(1 - \frac{1}{2}\Gamma\mu\right)P_H(\rho) + \Gamma\rho E; \quad \mu = \frac{\rho}{\rho_0} - 1 \tag{41}$$

where Γ is Gruneisen material parameter and P_H is Hugnoit pressure given by,

$$P_H(\rho) = \frac{C^2\mu(1+\mu)}{[1-\mu(S-1)]^2} \tag{42}$$

where C and S are the parameters in the linear shock velocity – particle velocity relationship $U_s = C + SU_p$. The plastic flow of the material is determined by the Von Mises criterion when the stress invariant exceeds the yield strength.

The damage model used in this simulation has been developed by Randles et al [18,19] and is generally considered suitable for treating impact fracture of Tungsten which may be combination of ductile and brittle mechanisms. This model uses a scalar damage variable without attempting to connect directly with microscopic mechanisms. The evolution of the scalar damage variable D with time is postulated as [18],

$$\frac{dD}{dt} = \frac{1}{\tau}\left[\frac{(\sigma_{\max} - \sigma_{th})}{\sigma_{th0}}\right]^2\left(\frac{1}{1-D^2}\right) \quad \sigma_{\max} > \sigma_{th} \tag{43}$$

where $\sigma_{\max}$ is the maximum principal stress, σ_{th} is the threshold stress for the onset of tensile damage, σ_{th0} is the threshold for undamaged material and τ is the time constant controlling the rate of damage growth. The accumulation of damage is zero when $\sigma_{\max} < \sigma_{th0}$. The damage variable ranges from 0 to 1 with 0 denoting no damage and, 1 complete damage with possible separation, and values in between denoting various states of damage between undamaged material and complete separation. The effects of damage evolution on material properties are given by [18],

$$\sigma_{th} = \sigma_{th0}(1-D^2) \quad k = k_0(1-D^2) \quad Y = Y_0(1-D^2) \quad G = G_0(1-D^2) \tag{44}$$

where k is tensile bulk modulus, Y is the yield stress for plastic deformation, and G is shear modulus. The k_0, Y_0 and G_0 are initial values of the corresponding material properties. The detail analysis of this damage model and its implementation can be found in the reference [18,19].

Material	$\rho_0(g/cc)$	C(mm/μs)	S	$G_0(Mb)$	Y_0(Kb)	Γ	σ_{th0}(Kb)	$\tau(\mu s)$
Tungsten	19.23	4.00	1.23	1.540	60.0	1.54	35.00	0.05
Silica Phenolic	1.71	3.24	1.39	0.038	10.0	1.00	2.00	0.50

Table 2. *Material Properties of Tungsten and Silica Phenolic*

The properties of materials used in the numerical simulations are listed in Table2 [18]. Figures (9.Ia) and (9.Ib) show the initial configurations of side and top views of the materials. And the Figures (9.Ia) and (9.Ib) show the views of the materials after the complete penetration of the Tungsten cube. The above initial set up is chosen in order to reduce the computational effort required. In the present example a penalty based contact-impact algorithm has been adopted [20,21].

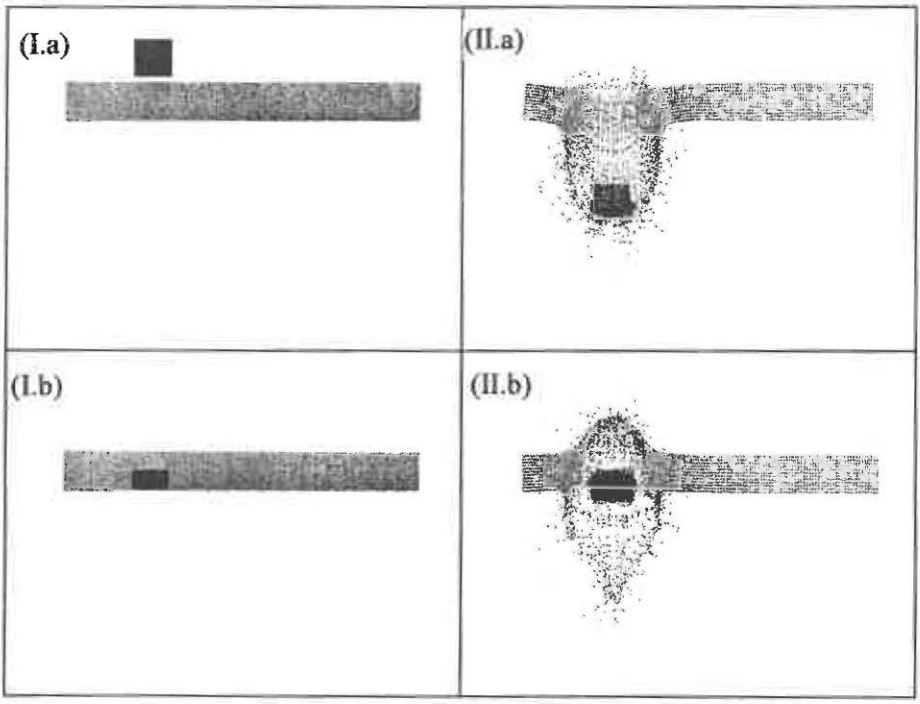

Figure 9. *Damage and Fracture of Tungsten cube and Silica-Phenolic bar*

5. Concluding remarks

It has been quoted in the literature that the tensile instability generally experienced in Eulerian based meshless techniques can be eliminated by using a Lagrangian kernel, i.e. by letting the kernel be a function of reference or initial configuration. This paper has discussed alternative Lagrangian SPH formulations to overcome the problem of such tensile instabilities. Two different formulations namely have been discussed at length. Remarkably, both Lagrangian expressions for the internal forces preserve linear and angular momentum given that in the case of corrected SPH the derivatives of the kernel at the reference configuration satisfy zero order completeness. As the derivative of kernel functions are fixed at the reference configuration the amount of computational effort here would be much less than that of Eulerian based meshless technique. Further, for the alternative Lagrangian SPH formulation presented, as the corrections are already included in the definition of the gradient functions, the computational cost can be further reduced. However, it is important to note that for problems involving large distortions, a Lagrangian formulation may require frequent updates of the reference configurations. Robust procedures for carrying out such updates are currently under investigation.

Finally the ability of the Lagrangian formulations to simulate complex problems is demonstrated by several numerical examples. All the numerical simulations are carried out in three spatial dimensions using total Lagrangian approach. The results obtained in the Taylor bar impact problem show close agreement with finite element simulations. The other simulations illustrate the possible potential applications of the Lagrangian SPH formulations.

Acknowledgements

This research has been funded by the Engineering and Physical Sciences Research Council (ESPRC) via grant number GR/L78352. This financial support is gratefully acknowledged.

6. References

1. L.B. Lucy, "A numerical approach to the Testing of the Fission Hypothesis", *Astro. J.*, 82, 1013 (1977)

2. R.A. Gingold and J. J. Monaghan, "Smooth Particle Hydrodynamics: Theory and Application to Non-Spherical Stars", *Mon. Not. R. Astron. Soc.*, 181, 375 (1977)

3. M. Schussler and D. Schmitt, Comments on Smoothed Particle Hydrodynamics, *Astron. Astrophys.*, 97, 373 (1981)

4. R.A. Gingold and J. J. Monaghan, "Kernel Estimates as a Basis for General Particle Methods in Hydrodynamics", *J. Comp. Phys.*, 46, 429 (1982)

5. J. J. Monaghan, "An Introduction to SPH", *Comput. Phys. Comm.* 48, 89-96 (1988)

6. L.D.Libersky, A.G.Petschek, T.C. Carney, J.R. Hipp, F.A.Allahadi, "High Strain Lagrangian Hydrodynamics", J.Comput. Phys., 109, 67 (1993)

7. W. Benz and E. Asphaug, "Simulations of Brittle Solids using Smooth Particle Hydrodynamics", Comput. Phys. Comm., 87, 253 (1995)

8. G.R. Johnson, R.A. Stryk, S.R. Beissel, "SPH for High Velocity Impact Computations", Comput. Methods Appl. Mech. Engrg., 139, 347 (1996)

9. W.K.Liu, S. Jun and Y.F. Zhang, "Reproducing Kernel Particle Methods", *Int. J. Num. Meth. Engrg.*, 20, 1081-1106, (1995).

10. J. Bonet and S. Kulasegaram, "Correction and Stabilization of Smooth Particle Hydrodynamics Methods with Applications in Metal Forming Simulations", *Int. J. Num. Meth. Engrg.*, 47, 1189-1214, (2000).

11. T. Belytschko, Y.Guo, W.K. Liu and S.P. Xiao, "A unified stability analysis of meshless methods", *Int. J. Num. Meth. Engrng.*, 48, 1359-1400, (2000).

12. J. Bonet and S. Kulasegaram, "Remarks on Tension Instability of Eulerian and Lagrangian Corrected Smooth Particle Hydrodynamics (CSPH) methods", *Int. J. Num. Mthds in Engrg.*, 52, 1203-1220, (2001).

13. J.W.Swegle, D.L. Hicks and S.W. Attaway, "Smooth Particle Hydrodynamics Stability Analysis", *J. Comp. Phys.* 116, (1995).

14. C.T Dyka, R.P. Ingel, "An approach for Tension Instability in Smooth Particle Hydrodynamics(SPH)", Computers & Structures 57, (1995).

15. C.T.Dyka, R.P. Ingel, "Stress Points for Tension Instability in SPH", *Int. J. Num. Meth. Engrng.* 40, 2325-2341, (1997).

16. J. Bonet and R. D. Wood, Non-linear Continuum Mechanics for Finite Element Analysis, Cambridge Uni. Press, Cambridge, UK (1997).

17. J. Bonet and A.J. Burton, "A Simple Average Nodal Pressure Tetrahedral Element for Incompressible and Nearly Incompressible Dynamic Explicit Application", *Comm. Numer. Meth. Eng.* 14 (5), 437-449, (1998).

18. P.W. Randles, T.C.Carney, L.D.Libersky, J.D.Renick, A.G. Petschek, "Calculation of Oblique Impact and Fracture of Tungsten Cubes Using Smoothed Particle Hydrodynamics" *Int. J. Imp. Engng.* 17, 661-672, (1995).

19. P.W. Randles and J.A. Nemes,"A Continuum Damage Model For Thick Composite Materials Subjected to High-Rate Dynamic Loading", *Mechanics of Materials* 13(1), 1-13, (1992).

20. T. Belytschko and M. O. Neal, "Contact-Impact by the Pinball Algorithm with Penalty and Lagrangian Methods", *Int. J. Num. Mthds. in Engrg.* 31, pp.547-572, (1991).

21. R. Vignjevic, J.Campbell, L. Libersky, "A Treatment of Zero-Energy modes in the Smoothed Particle Hydrodynamics Method", *Comput. Methods. Appl. Mech. Engrg.* 184, 67-85, (2000).